Prediction method of radial heat affected zone width in nanosecond pulsed laser ablation of TC4

Xulin Wang
Zhenyuan Jia
Jianwei Ma (mjw2011@dlut.edu.cn)
Dalian University of Technology
Dongxu Han
Xiaoqian Qi
Chuanheng Gui
Wei Liu

Research Article

Keywords: Nanosecond pulsed, Micromachining, Heat-affected zone, Microgroove, TC4, Temperature distribution

Posted Date: March 18th, 2022

DOI: https://doi.org/10.21203/rs.3.rs-1442005/v1

Prediction method of radial heat affected zone width in nanosecond pulsed laser ablation of TC4

Xulin Wang[1] · Zhenyuan Jia[1] · Jianwei Ma[1] · Dongxu Han[1] · Xiaoqian Qi[1] · Chuanheng Gui[1] · Wei Liu[1]

Abstract

Nanosecond pulsed laser ablation (NPLA) is widely used in micromachining. However, during the machining process, the radial heat-affected zone (RHAZ) will deteriorate the machining quality and accuracy of the microgroove, which is the basic unit of the ridge surface used to reduce frictional resistance in spacecraft walls. Its effective prediction is crucial for the processing precision control of microgrooves to ensure the drag reduction performance of the ridge surface. For this reason, this paper proposes an effective method to predict the RHAZ width. TC4, commonly used in aerospace, is the target material in this work. By comprehensively considering the thermal accumulation effect of laser pulses and the superimposability of the temperature field, and based on the point heat source method, a dynamic temperature distribution model in NPLA is established. Then, the RHAZ width is initially predicted by combining the graphical method and the RHAZ definition. Finally, to improve the prediction accuracy of the RHAZ width. A correction factor is obtained by the NPLA of microgrooves on TC4. The relative error between the predicted RHAZ width and observed values is less than 7% after introducing the correction factor, which verifies the reliability and validity of the proposed prediction method for the RHAZ width. Furthermore, the RHAZ width in NPLA of TC4 is on the order of hundreds of microns, which should be considered to ensure its processing quality when the ridge surface is designed on TC4. The research method in this paper will guide the design of high-density functional patterns and their high-precision preparation and has significant engineering practical value.

Keywords Nanosecond pulsed · Micromachining · Heat-affected zone · Microgroove · TC4 · Temperature distribution

1 Introduction

Nanosecond pulsed laser ablation (NPLA) has the advantages of high processing accuracy and environmental protection compared with traditional processing [1-3]. Meanwhile, compared with picosecond and femtosecond lasers, nanosecond lasers have a lower cost [4]. So, a nanosecond laser can achieve the efficient and low-cost manufacturing of the microgroove that is the basic unit of the ridge surface used to reduce frictional resistance in spacecraft walls [2, 5]. However, the commonly used material in aerospace is TC4 with low thermal conductivity [6]. The NPLA of TC4 will produce the apparent radial heat-affected zone (RHAZ), limiting the high-precision preparation of microgrooves [2]. Therefore, the effective prediction of the RHAZ width is crucial for the processing precision control of microgrooves to ensure the drag reduction performance of the ridge surface.

✉ Jianwei Ma
mjw2011@dlut.edu.cn

[1] Key Laboratory for Precision and Non-traditional Machining Technology of the Ministry of Education, School of Mechanical Engineering, Dalian University of Technology, Dalian 116024, China

Simulation and optimized methods have predicted the RHAZ width in the laser processing. Valette et al. [7] developed a 2D temperature model and predicted the RHAZ width of nanosecond laser ablating aluminum. The predicted results are in reasonable agreement with experimental results. However, the presented model cannot strictly simulate experiments since it considers only a single pulse. Mishra et al. [8] developed an axisymmetric finite element (FE) model to determine the transient temperature distribution in the aluminum sheet, which is further used to determine the RHAZ width. Yang et al. [9] proposed a 3D transient FE model for moving Gaussian laser heat sources to predict the RHAZ width on TC4. Successively, many scholars developed 3D FE models for RHAZ width prediction [10-13]. Furthermore, the response surface method was used to establish the functional relationship between laser processing parameters and the RHAZ width. Based on the established functional relationship, the RHAZ width was predicted [14, 15]. In recent years, the research of intelligent algorithms has set off an upsurge in academia, such as genetic algorithms [16, 17], artificial neural networks [18], adaptive neuro-fuzzy techniques [19], extreme learning machines [20, 21], etc. They predicted the RHAZ width well in laser processing.

The above research has contributed to predicting RHAZ width during laser processing. However, there are still problems such as low efficiency of simulation calculation, high experimental cost of optimization methods based on experimental data, and insufficient theoretical method for predicting the RHAZ width of NPLA. Therefore, the purpose of this paper is to propose an efficient and low-cost method for predicting the RHAZ width in NPLA of microgrooves on TC4, which will realize the high-precision manufacturing of the ridge surface to reduce frictional resistance in spacecraft walls. The innovation is based on the NPLA mechanism of metal and the point heat source method to derive the dynamic temperature distribution model on the target material. And the RHAZ width is predicted initially based on the temperature distribution chart and the RHAZ definition. By introducing a correction factor to reduce the prediction error caused by model simplification, the prediction accuracy of the RHAZ width is finally improved.

2 Prediction method of RHAZ width in NPLA of microgroove on TC4

In response to the existing problems of the RHAZ prediction study in Part 1, with the vital help of previous studies, this part proposes an effective method for predicting the RHAZ width in NPLA of microgrooves (as shown in Fig. 1). Specifically, since the NPLA of metals is highly complicated, some assumptions are first made to simplify calculations. Then, by solving the electric field distribution equation of the fundamental mode Gaussian beam, combining the relationship between the laser energy distribution and the electric field distribution, the laser energy distribution on the workpiece surface is obtained. And based on the energy conservation equation and the static instantaneous point heat source, the point heat source is further derived. Then, the deduced point heat source is integrated over the entire laser spot. The temperature rise at which the single-pulse laser acts on the workpiece surface under steady-state conditions is obtained. Next, the laser spot (circular heat source) is simplified as a point heat source. Combined with the dynamic instantaneous point heat source, the dynamic instantaneous point heat source under the action of a single pulse is obtained. After that, considering the thermal accumulation effect of laser pulses and the superimposability of the temperature field, the dynamic temperature distribution model of the multi-pulse laser is obtained. Finally, based on the graphical method and the RHAZ definition, the RHAZ width is effectively predicted by introducing a correction factor. The detailed solution process of the RHAZ width is as follows.

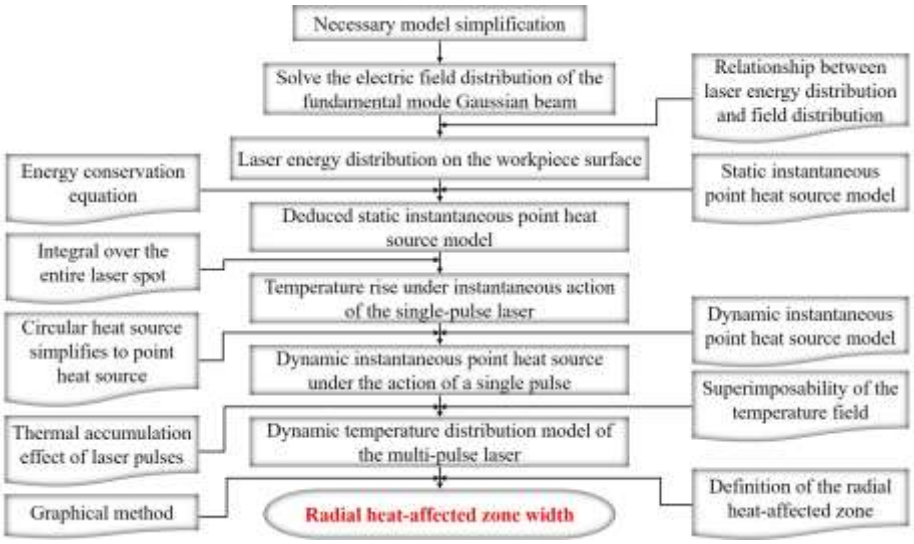

Fig. 1 Prediction methodology of the RHAZ width

The thermal process for the NPLA of metals is very complicated. Some assumptions are as follows to simplify the calculation.

- Since the laser spot size is much smaller than the workpiece size and the heat penetration distance is almost zero, the workpiece is regarded as a semi-infinite object.
- The material is isotropic, and the physical properties are constant.
- The effects of convection, radiation, sputter, and plasma are not considered.
- Laser energy obeys Gaussian distribution.

When the laser is incident on the workpiece surface, the electric field distribution of fundamental mode Gaussian beam propagating along the *Z*-axis can be expressed as [22]

$$\psi_{00}(x,y,z)=\frac{a}{w(z)}e^{-\frac{r^2}{w^2(z)}-i\left[k\left(z+\frac{r^2}{2R(z)}\right)-arctg\frac{z}{f_0}\right]} \tag{1}$$

Where a is a constant, $w(z)$ is the radius of the laser spot, r is the distance between the coordinate point in the plane perpendicular to the Z-axis and the center of the spot. $R(z)$ is the curve radius at the coordinate point Z along the beam propagation direction. f_0 is the confocal parameter of the Gaussian beam. $k=2\pi/A$. A is the laser wavelength, and i is an imaginary unit.

The energy distribution is proportional to the square of the amplitude for the electric field distribution [22]. Thus, according to Eq. (1), the energy distribution $I(r)$ acting on the plane of the vertical propagation direction can be expressed as

$$I(r)=\frac{b}{w^2}e^{-2\frac{r^2}{w^2}} \tag{2}$$

Where b is a constant and w is the spot radius of the laser beam on the workpiece surface.

Furthermore, the incident laser is reflected, absorbed, and transmitted on the workpiece surface, conforming to energy conservation. This process can be expressed as

$$I_0=I_R+I_\alpha+I_T \tag{3}$$

Where I_0 is the total energy incident on the workpiece surface, and I_R is the energy reflected by the workpiece surface. I_α is the energy absorbed by the workpiece, and I_T is the energy remaining by the laser through the material.

Since the laser cannot pass through opaque materials, I_T can be expressed as

$$I_T = 0 \tag{4}$$

When the laser power incident on the workpiece surface is P, according to Eq. (3) and Eq. (4), the energy conservation equation can be expressed as

$$P(1-R)/f = \iint_S I(r)dS \tag{5}$$

Where R is the reflectivity of material, f is the laser frequency, S is the surface area of the workpiece.

According to Eq. (2) and Eq. (5), the energy distribution $I(r)$ on the workpiece surface under the action of the single-pulse laser can be obtained by

$$I(r) = \frac{2P(1-R)}{f\pi w^2} \mathrm{e}^{-2\frac{r^2}{w^2}} \tag{6}$$

Based on the point heat source method, the static instantaneous point heat source $T(r, t)$ can be expressed as [23]

$$T(r,t) = \frac{I_0}{4c\rho(\pi\alpha t)^{3/2}} \mathrm{e}^{-\frac{r^2}{4\alpha t}} \tag{7}$$

Where I_0 is the energy density at the center of the spot, c, ρ, λ, α is the specific heat, density, thermal conductivity, thermal diffusivity of the material, respectively. t is the time. $\alpha=\lambda/(c\rho)$.

Combining Eq. (6) and Eq. (7), $T(r, t)$ is derived as

$$T(r,t) = \frac{P(1-R)}{2f\pi w^2 c\rho(\pi\alpha t)^{3/2}} \mathrm{e}^{-\frac{r^2}{4\alpha t}} \tag{8}$$

Since the laser spot is a circular surface source [23], the temperature rise T_0 at which the single-pulse laser acts on the workpiece surface under steady-state conditions can be obtained by solving the surface integral of Eq. (8) over the entire laser spot.

$$T_0 = \iint_S dS \int_0^{+\infty} \frac{P(1-R)}{2f\pi w^2 c\rho(\pi\alpha)^{3/2}} t^{-3/2} \mathrm{e}^{-\frac{r^2}{4\alpha t}} dt \tag{9}$$

Solving Eq. (9) to get

$$T_0 = \frac{2P(1-R)}{\pi f \lambda w} \tag{10}$$

In the following study, the laser spot is considered a point heat source to simplify the calculation. And NPLA is equivalent to a combination of a series of moving point heat sources [23]. It is assumed that the point heat source moves at the velocity v along X-axis, after the time t, the coordinate of the point heat source is (x', y')

$$\begin{cases} x' = vt \\ y' = 0 \end{cases} \tag{11}$$

Dynamic instantaneous point heat source can be expressed as [24]

$$T(x, y, t) = \frac{T_0}{8(\pi\alpha t)^{2/3}} \mathrm{e}^{-\frac{(x-x')^2+(y-y')^2}{4\alpha t}} \tag{12}$$

Bringing Eq. (10) and Eq. (11) into Eq. (12), the dynamic instantaneous point heat source under the action of a single pulse is obtained by

$$T_{monopulse}(x,y,t)=\frac{P(1-R)}{4\pi^{5/3}fw\lambda(\alpha t)^{2/3}}\mathrm{e}^{-\frac{(x-vt)^2+y^2}{4\alpha t}} \tag{13}$$

There is a thermal accumulation effect between the laser pulses in NPLA [25]. According to the superimposability of the temperature field, the dynamic temperature distribution model of the multi-pulse laser is obtained by

$$T_{multipulse}(x,y,t,f,N)=T_r+\sum_{n=1}^{N}T_{monopulse}\left(x,y,t-\frac{n-1}{f}\right)\cdot H\left(t-\frac{n-1}{f}\right) \tag{14}$$

Where H is the unit step function, n is the number of pulses, N is the total number of pulses required for the NPLA [26], T_r is the room temperature, 293.15 K.

By solving Eq. (14), the temperature distribution on one side of the NPLA path at different times (such as t_1, t_2, t_3, t_4, t_5) is obtained, as shown in Fig. 2. Fig. 2 shows that the temperature distribution curves at different times are part of the Gaussian curve. T_m is the melting temperature of the metal, and T_a is the temperature of thermal activation ($T_a \approx 0.4T_m$) [7]. Moreover, it can be seen from the figure that the lateral coordinate y (the radial direction of the laser beam) can be expressed as the function of T and t.

$$y=f(T,t) \tag{15}$$

Finally, according to the definition of the RHAZ width that is the distance between the two points corresponding to T_m and T_a [7], combing the Fig. 2 and Eq. (15), and a correction factor ξ (ξ is obtained by the experiment) is introduced to reduce the prediction error of RHAZ width caused by model simplification, the RHAZ width W can be expressed as

$$W=\xi\cdot\left[f(T_a,t_3)-w\right] \tag{16}$$

Where $f(T_a,t_3)$ is the key to solving W, in Fig. 2, by adjusting t so that the temperature distribution curve is tangent to the T_m horizontal line, the temperature distribution curve corresponding to t_3 is obtained. The abscissa of the intersection of the above curve and the T_a horizontal line is $f(T_a,t_3)$.

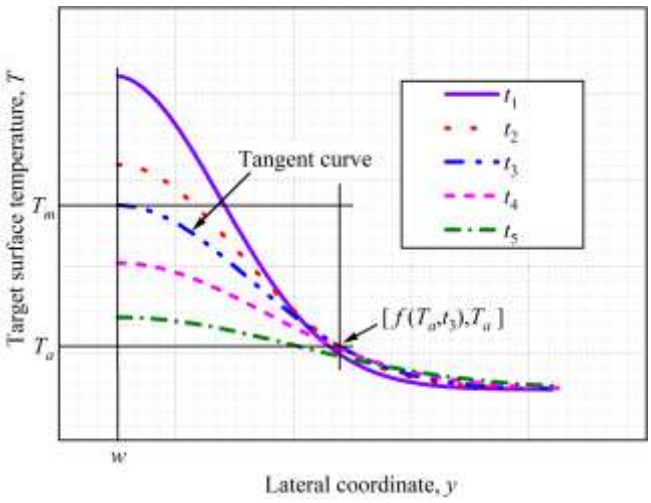

Fig. 2 Temperature distribution of NPLA at different times

3 Experiment

NPLA of microgrooves on TC4 is implemented to verify the validity and reliability of the method proposed in Part 2. The surface roughness of the polished TC4 is less than 0.3μm, which will not affect

the observation of laser processing morphology. The polished TC4 specimen is shown in Fig. 3. The thermophysical parameters of TC4 are shown in Table 1 [6].

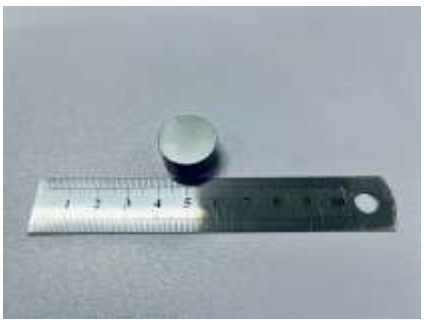

Fig. 3 Polished TC4 specimen

Table 1 Thermophysical parameters of TC4

Parameter	Symbol	Unit	Value
Thermal conductivity	λ	W/(m·K)	37
Specific heat	c	J/(kg·K)	850
Density	ρ	kg/m^3	3780
Melting temperature	T_m	K	1923
Vaporization temperature	T_v	K	3315
Latent heat of evaporation	L_v	J/kg	9.83×10^6
Reflectivity	R	1	0.76

Fig. 4 is the schematics of the NPLA setup used in experiments. The nanosecond laser beam is focused on the TC4 surface through a focusing lens, and its parameters are shown in Table 2. Then, the NPLA of microgrooves is realized by the movement of the workbench. Table 3 shows the NPLA parameters of microgrooves on the TC4 surface. The parameters in the table are determined based on our previous single-factor experiments (the power and velocity are the key parameters that affect the RHAZ [9, 10, 13, 15, 19]). 20kHz makes the RHAZ significant while ensuring the generation of microgrooves better to verify the validity of the RHAZ prediction method. Finally, an optical microscope can measure the RHAZ on one side of the microgroove. The experimental RHAZ width W' can be expressed as

$$W' = \frac{W_2 - W_1}{2} \tag{17}$$

Where W_1 is the experimental value of the microgroove width, W_2 is the distance between the outer boundaries of the RHAZ.

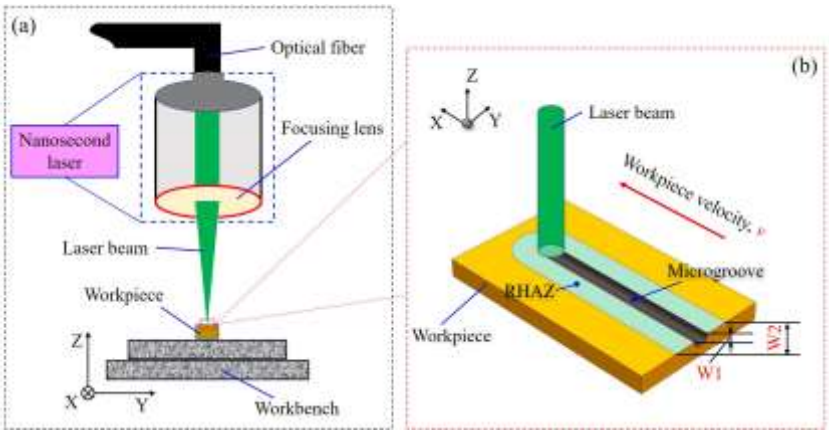

Fig. 4 Schematics of the NPLA setup used in experiments. (a) NPLA setup. (b) NPLA of microgrooves on TC4 Surface

Table 2 Nanosecond laser parameters

Parameter	Symbol	Unit	Value
Wavelength	A	nm	532
Pulse width	τ	ns	15
Spot radius	w	μm	20

Table 3 Laser processing parameters

Parameter	Symbol	Unit	Values
Power	P	W	2.1, 3.1, 4.2, 5.7, 6.8
Frequency	f	kHz	20
Velocity	v	m/min	3, 3.5, 4, 4.5, 5

4 Experimental verification

4.1 Determination of correction factor

In this part, the correction factor of Part 2 is obtained experimentally to improve the prediction accuracy of the RHAZ. Fig. 5 shows the measurement of W_1 and W_2 under different power (processing parameters: 2.1W, 3.1W, 4.2W, 5.7W, 6.8W, 3m/min, 20kHz). Based on the first three sets of data in the figure and Eq. 17, Table 4 is calculated. We take the average of the ratios of the uncorrected W to the observed W' as the correction factor.

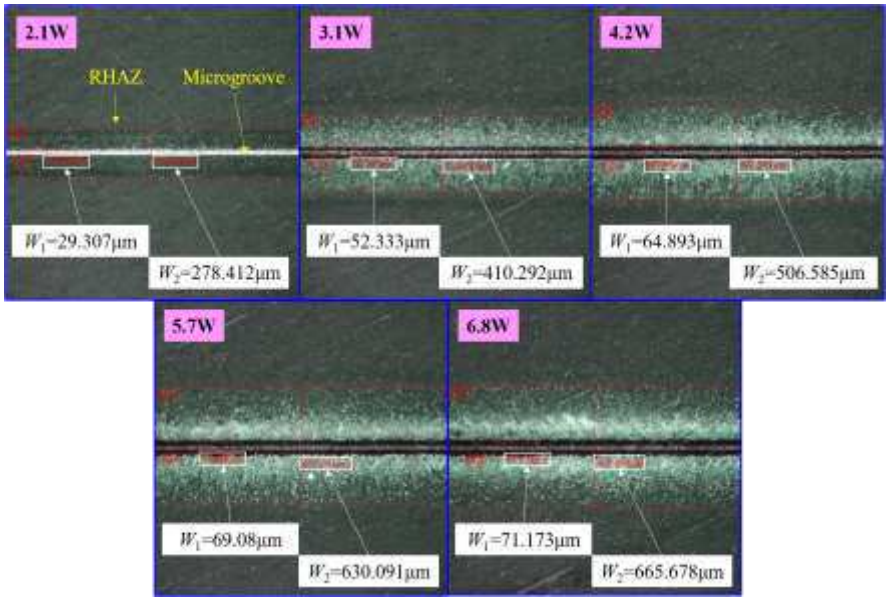

Fig. 5 Measurement of W_1 and W_2 under different power. Processing parameters: 2.1W, 3.1W, 4.2W, 5.7W, 6.8W, 3m/min, 20kHz

Table 4 Determination of correction factor

P (W)	f (kHz)	v (m/min)	Uncorrected W (μm)	W' (μm)	W/W'	ξ
2.1	20	3	404.57	124.553	3.25	
3.1	20	3	560.849	178.98	3.13	(3.25+3.13+3.15)/3=3.18
4.2	20	3	696.759	220.846	3.15	

4.2 Verification of RHAZ width predicted method

After introducing the correction factor, the RHAZ width is re-solved. The experimental observation and prediction results are shown in Fig. 6, Fig. 7, and Fig. 8.

Fig. 6 is the effect of power on the RHAZ width (processing parameters: 2.1W, 3.1W, 4.2W, 5.7W, 6.8W, 3m/min, 20kHz). It can be seen from the figure that both predicted and experimental values of RHAZ width increase with power. The above rule is related to the fact that the laser energy absorbed by the target increases with the increase of power, and then the thermal diffusion distance increases [27]. Furthermore, the relative error between predicted and observed values is less than 4%. Fig. 7 is the measurement of W_1 and W_2 under different velocity (processing parameters: 3m/min, 3.5m/min, 4m/min, 4.5m/min, 5m/min, 6.8W, 20kHz). From the data in Fig. 7, the effect of velocity on the RHAZ width in Fig. 8 is obtained. Fig. 8 shows that both predicted and experimental values of the RHAZ width decrease with increasing speed. It is related to the fact that the spot overlap coefficient decreases with the speed increase, decreasing laser energy absorbed by the target, which weakens the thermal diffusion [27]. In addition, the relative error between predicted and observed values is less than 7%. Therefore, the above results verify the validity and reliability of the RHAZ width prediction method proposed in this paper. Further, according to Fig. 6 and Fig.8, low power and high speed are beneficial to shrink the RHAZ, and the RHAZ width ranges from 125μm to 300μm within the processing parameters studied in this paper. It will guide the design of the groove spacing of the ridge surface on TC4 in the NPLA to ensure its machining accuracy.

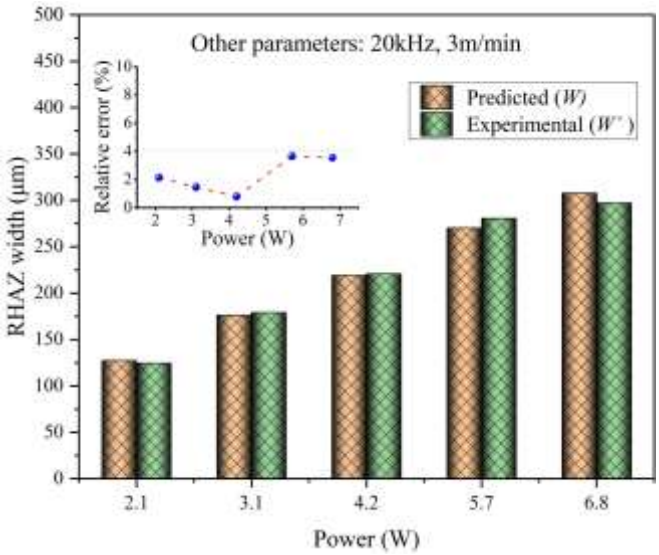

Fig. 6 Effect of power on the RHAZ width. Processing parameters: 2.1W, 3.1W, 4.2W, 5.7W, 6.8W, 3m/min, 20kHz

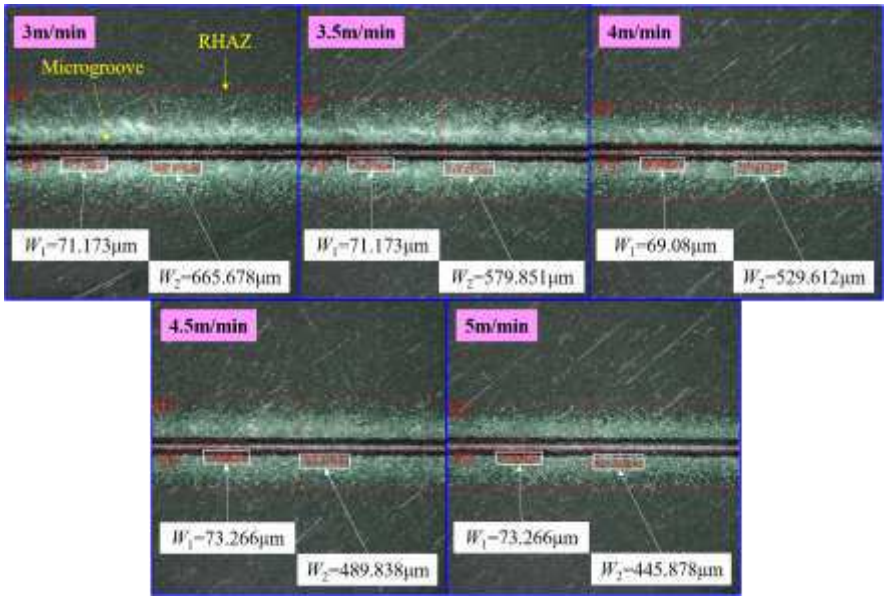

Fig. 7 Measurement of W_1 and W_2 under different velocity. Processing parameters: 3m/min, 3.5m/min, 4m/min, 4.5m/min, 5m/min, 6.8W, 20kHz

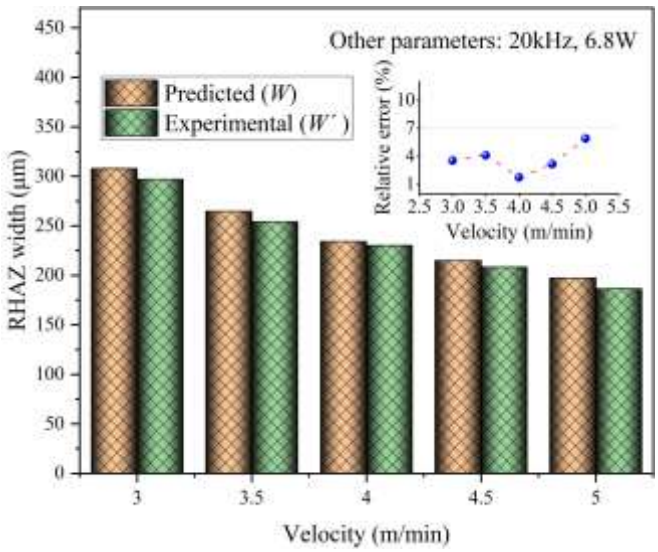

Fig. 8 Effect of velocity on the RHAZ width. Processing parameters: 3m/min, 3.5m/min, 4m/min, 4.5m/min, 5m/min, 6.8W, 20kHz

5 Conclusions

In our research, an efficient and low-cost method for predicting the RHAZ width in NPLA of microgrooves on TC4 is proposed and verified by experiments. During our research process, some conclusions are as follows:

(1) The relative error between the predicted RHAZ width and the experimental value is less than 7%, which verifies the effectiveness and reliability of the proposed method. Furthermore, the low power and high speed are beneficial to shrink the RHAZ.

(2) Within the parameters studied, the RHAZ width in NPLA of TC4 is on the order of hundreds of microns.

(3) The proposed method will guide the design of high-density functional patterns and their high-precision preparation and has significant engineering practical value.

Author contribution Xulin Wang: methodology, formula derivation, writing-original draft. Zhenyuan Jia: project administration, conceptualization, writing-review and editing. Jianwei Ma: project administration, conceptualization, writing-review and editing. Dongxu Han: formula derivation, verification. Xiaoqian Qi: data analysis, grammar and format. Chuanheng Gui: programming calculation, grammar and format. Wei Liu: project administration.

Funding This work is supported by National key research and development plan of China (No. 2018YFA0703304), National Natural Science Foundation of China (No. 51975098 and U1937602), Liaoning Revitalization Talents Program (No. XLYC1907006, XLYCYSZX1901, XLYC1801008), and Fundamental Research Funds for the Central Universities.

Availability of data and material The data presented in this study are available upon request to the corresponding author. All the data is presented within the article.

Code availability The code used to obtain the predicted results in this study is available upon request to the corresponding author.

Declarations

Ethics approval The authors confirm that this manuscript has not been submitted to other journals, is not previously published, or in press. The authors confirm that all the presented information is original.

Consent to participate Not applicable.

Consent for publication All authors have read and agreed to the published version of the manuscript.

Conflict of interest The authors declare that they have no known competing financial interests or personal relationships that could have appeared to influence the work reported in this paper.

References

1. Wahab JA, Ghazali MJ, Yusoff WMW, Sajuri Z (2016) Enhancing material performance through laser surface texturing: a review. Trans Inst Metal Finish 94(4):193-198. https://doi.org/10.1080/00202967.2016.1191141
2. Han YY, Zhang ZP, Qu LT (2019) Laser-induced structured biomimetic surface. Chinese Science Bulletin 64(12):1238-1253. https://doi.org/10.1360/N972018-00855
3. Zhang BY, Di YL, Wang HD, Kang JJ, Liu T (2020) Research progress in preparation of super-hydrophobic surface of metal matrix by laser processing. Materials Review 34(12):23109-23120
4. Nedyalkov N, Dikovska A, Aleksandrov L, Terakawa (2021) Nanosecond laser ablation of AlN ceramic. Appl Phys A-Mater Sci Process 127(12):951. https://doi.org/10.1007/s00339-021-05106-3
5. Wang CJ, Cheng LD, Xue SX, Chen PY, Liu BS, Ding H, Sun J, Xu ZH, Wang XW (2019) Manufacturing technologies of bionic micro-structures for drag reduction: a review. J Nets Form Eng 11(3):88-98. https://doi.org/10.3969/j.issn.1674-6457.2019.03.009
6. Wang XL, Jia ZY, Ma JW, Han DX, Gui CH, Qi XQ, Liu W (2022) Research on simulation of nanosecond pulsed laser processing for TC4 titanium alloy: A novel model simplification and correction method. Opt Laser Technol 147:107635. https://doi.org/10.1016/j.optlastec.2021.107635
7. Valette S, Le Harzic R, Huot N, Audouard E, Fortunier R (2005) 2D calculations of the thermal effects due to femtosecond laser-metal interaction. Appl Surf Sci 247(1-4):238-242. https://doi.org/10.1016/j.apsusc.2005.01.080
8. Mishra S, Yadava V (2013) Modelling of hole taper and heat affected zone due to laser beam percussion drilling. Mach Sci Technol 17(2):270-291. https://doi.org/10.1080/10910344.2013.780554
9. Yang JH, Sun SJ, Brandt M, Yan WY (2010) Experimental investigation and 3D finite element prediction of the heat affected zone during laser assisted machining of Ti6Al4V alloy. J Mater Process Technol 210(15):2215-2222. https://doi.org/10.1016/j.jmatprotec.2010.08.007
10. Zhai CT, Xu JK, Li YQ, Hou YG, Yuan SS, Wang X, Liu QM (2020) Study on surface heat-affected zone and surface quality of Ti-6Al-4V alloy by laser-assisted micro-cutting. Int J Adv Manuf Technol 109(7-8):2337-2352. https://doi.org/10.1007/s00170-020-05794-w
11. Tamrin KF, Moghadasi K, Sheikh NA (2020) Experimental and numerical investigation on multi-pass laser cutting of natural fibre composite. Int J Adv Manuf Technol 107(3-4):1483-1504. https://doi.org/10.1007/s00170-020-05121-3
12. Keivanloo A, Naffakh-Moosavy H, Miresmaeili R (2021) “The effect of pulsed laser welding on hot cracking susceptible region size and weld pool internal geometry of Inconel 718: Numerical and experimental approaches. CIRP J Manuf Sci Technol 35:787-794. https://doi.org/10.1016/j.cirpj.2021.09.001
13. Kholoud MJ, Akbari M, (2021) Numerical investigation of molten pool dimension, temperature field and melting flow during pulsed laser welding of Ti-6Al-4V alloy sheets with different thicknesses. J Laser Appl 33(3):032012. https://doi.org/10.2351/7.0000436

14. Bharatish A, Murthy HNN, Anand B, Madhusoodana CD, Praveena GS, Krishna M (2013) Characterization of hole circularity and heat affected zone in pulsed CO_2 laser drilling of alumina ceramics. Opt Laser Technol 53:22-32. https://doi.org/10.1016/j.optlastec.2013.04.010
15. Khoshaim AB, Elsheikh AH, Moustafa EB, Basha M, Showaib EA (2021) Experimental investigation on laser cutting of PMMA sheets: Effects of process factors on kerf characteristics. J Mater Res Technol-JMRT 11:235-246. https://doi.org/10.1016/j.jmrt.2021.01.012
16. Abdo BMA, El-Tamimi AM, Anwar S, Umer U, Alahmari AM, Ghaleb MA (2018) Experimental investigation and multi-objective optimization of Nd:YAG laser micro-channeling process of zirconia dental ceramic. Int J Adv Manuf Technol 98(5-8):2213-2230. https://doi.org/10.1007/s00170-018-2374-2
17. Jain A, Singh B, Shrivastava Y (2020) Analysis of heat affected zone (HAZ) during micro-drilling of a new hybrid composite. Proc Inst Mech Eng Part C-J Eng Mech Eng Sci 234(2):620-634. https://doi.org/10.1177/0954406219877911
18. Mehrpouya M, Gisario A, Huang H, Rahimzadeh A, Elahinia M (2019) Numerical study for prediction of optimum operational parameters in laser welding of NiTi alloy. Opt Laser Technol 118:159-169. https://doi.org/10.1016/j.optlastec.2019.05.010
19. Petkovic D, Nikolic V, Milovancevic M, Lazov L (2016) Estimation of the most influential factors on the laser cutting process heat affected zone (HAZ) by adaptive neuro-fuzzy technique. Infrared Phys Technol 77:12-15. https://doi.org/10.1016/j.infrared.2016.05.005
20. Anicic O, Jovic S, Skrijelj H, Nedic B (2017) Prediction of laser cutting heat affected zone by extreme learning machine. Opt Lasers Eng 88:1-4. https://doi.org/10.1016/j.optlaseng.2016.07.005
21. Nguyen TH, Lin CK, Tung PC, Nguyen-Van C, Ho JR (2020) An extreme learning machine for predicting kerf waviness and heat affected zone in pulsed laser cutting of thin non-oriented silicon steel. Opt Lasers Eng 134:106244. https://doi.org/10.1016/j.optlaseng.2020.106244
22. Wang GW, Zhang HZ (2017) Research on modeling of heat source based on laser energy distribution and its simulation application. Dissertation, Harbin Institute of Technology
23. Tan H, Shang WX, Zhang FY, Clare AT, Lin X, Chen J, Huang WD (2018) Process mechanisms based on powder flow spatial distribution in direct metal deposition. J Mater Process Technol 254:361-372. https://doi.org/10.1016/j.jmatprotec.2017.11.026
24. Steen WM (2012) Laser material processing. China Machine Press
25. Cha D, Axinte D (2021) Transient thermal model of nanosecond pulsed laser ablation: Effect of heat accumulation during processing of semi-transparent ceramics. Int J Heat Mass Transf 173:121227. https://doi.org/10.1016/j.ijheatmasstransfer.2021.121227
26. Zhao K, Jia ZY, Ma JM, Liu W, Wang L (2014) Nanosecond multi-pulse laser milling for certain area removal of metal coating on plastics surface. Opt Lasers Eng 63:58-69. https://doi.org/10.1016/j.optlaseng.2014.06.009
27. Jia ZY, Zhao K, Liu W, Ma JW, Wang L (2014) Nanosecond pulsed laser processing circuits on the copper clad polyimide. Int J Machining and Machinability of Materials 15(3-4):157-173. https://doi.org/10.1504/IJMMM.2014.060547